Edge extraction and reconstruction of terahertz image using simulation evolutionary with the symmetric fourth order partial differential equation*

PAN Xue-wen (潘学文)[1], **ZHAO Quan-you** (赵全友)[1], **and LIU Jian-jun** (刘建军)[2]**

1. School of Electronics and Information Engineering, Hunan University of Science and Engineering, Yongzhou 425199, China

2. School of Intelligent Engineering, Shaoguan University, Shaoguan 363000, China

(Received 12 May 2020; Revised 12 August 2020)

Terahertz (THz) pulse imaging can be used for biomedicine, material, and food security. However, image quality is lower attributed to the THz time-domain spectroscopy system. Such as, noises and lower space resolution are presented in some THz images. To improve the THz image quality, we proposed a novel method which combining the simulation evolutionary with the symmetric fourth order partial differential equation. The image edge is first detected by using the simulation evolutionary. Then the symmetric fourth order partial differential equation (PDE) is applied on the non-edge image for noise reduction. Finally, the de-noise image is combined with the edge image obtained from the edge detection step. Experiments on four different THz images prove that the proposed method can preserve the edge information during noise reduction.

Document code: A **Article ID:** 1673-1905(2021)03-0187-6

DOI https://doi.org/10.1007/s11801-021-0080-z

Terahertz (THz) is an electromagnetic wave with the frequency ranging from 0.1 THz to 10 THz, where 1 THz=10^{12} Hz, corresponding to a wavelength range of 3 mm to 30 μm, and terahertz pulse imaging (TPI) is a non-invasive coherent optical image modality using electromagnetic radiation[1]. TPI have aroused intense interests due to their potential applications in biomedical, nondestructive imaging of packages, trace gas analysis, inspection of artworks and counterfeit note, and semiconductor device diagnostics[2-5]. Generally, THz imaging technology including coherent imaging and non-coherent imaging, the former typically contains time-domain spectroscopy imaging, electro optics imaging and chromatography imaging, yet continuous wave imaging usually belongs to the latter[6,7]. Currently, TPI investigation mainly involves two aspects. On the one hand, many researchers focus on how to overcome the obstacles in hardware, i.e., how to improve the resolution, accuracy and speed in TPI system[8-10]. On the other hand, to further improve the quality of images obtained from THz system, a few digital image processing methods have been introduced[1].

Images obtained by THz technique are sometimes not clear enough to distinguish the profile and the edge of the sample. What is more, they also affected by speckle noises that will reduce the recognition accuracy of the object. Therefore, de-noising becomes a key step during THz image processing. However, classical digital image de-noising methods, such as mean filter, median filter and non-local means (NLM)[11] will blur the image edge when reducing the noises. Therefore, development of a feasible and effective de-noising method is of great importance for the theoretical study of THz images.

Recently, the fourth order partial differential equation (PDE) has been introduced into image de-noising study[12]. It can achieve a good trade-off between noise removal and edge preservation. In addition, simulation evolutionary has also been proved to be more effective than traditional edge detection operators (such as Sobel and Canny) in image edge detection[13,14]. Simulation evolutionary is a swarm-based meta-heuristic inspired by the foraging behavior of some ant species in nature. Through several ants in a movement driven by the local variation of the image's intensity values, a pheromone matrix corresponding to the edge information at each pixel location in the image can be established[15].

Based on the pioneering studies mentioned above, to presser the edge information during noise removal, we

* This work has been supported by the Hunan Provincial Natural Science Foundation Program (No.2020JJ4327), the Department of Education Science Research General Project in Hunan Province (No.18C1063), the Featured Application Discipline in Hunan University of Science and Engineering (Computer Science and Technology), the Scientific Research Projects in Colleges and Universities (No.2019KTSCX165), and the Shaoguan Science and Technology Department Project (No.2019sn066).

** E-mail: 37644313@qq.com

proposed that combine the symmetric fourth order PDE with the simulation evolutionary. Firstly, simulation evolutionary is used to detect the image edge. Then, a few ants are utilized to move on a two-dimensional (2D) image for constructing a pheromone matrix. Thirdly, the symmetric fourth order PDE is applied to reduce the noises on non-edge image. Finally, the de-noise non-edge image and edge image are combined to reconstruct the result. In this paper, we describe how to obtain the THz images through the experimental apparatus. The simulation evolutionary for edge detection and the symmetric fourth order PDE de-noise approach are presented. The calculated results and the related discussion are presented.

The THz-time-domain spectroscopy system used in this article is a transmission time-domain spectroscopy detection system, as shown in Fig.1.

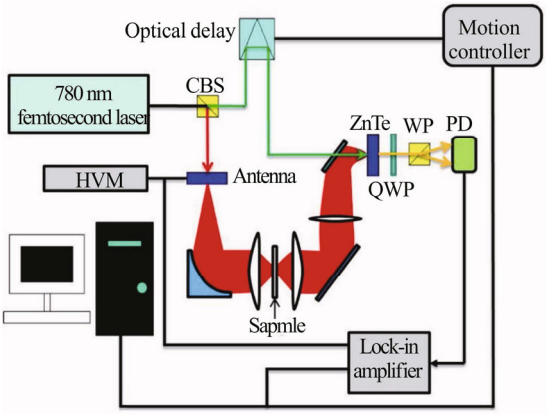

Fig.1 The schematic diagram of THz-TDS system

The apparatus consists of two parts: the Z-3 THz time-domain spectrometer (Zomega Terahertz Corp., USA), and the femtosecond laser, FemtoFiber pro NIR (TOPTICA Photonics Inc., Germany). The femtosecond laser is used as a radiation source. It has 780 nm central wavelength, 100 fs pulse width, 80 MHz repetition rate and nearly 140 mW average power. The laser beam is divided into the pump light (nearly 96 mW) and the probe light (about 16 mW) by a cubic beam splitter (CBS) for THz generation and detection, respectively. The whole experimental system has a spectral resolution of less than 5 GHz and a dynamic range of better than 70 dB. To avoid the interference of water vapor in the ambient air, the apparatus was placed in a closed box and dry air was injected until the indoor relative humidity (RH) is less than 2%.

Owing to the edge information is vital for THz image processing, to preserve the edge information during de-noising process we proposed combining the simulation evolutionary with symmetric fourth order PDE. Edge detection is first conducted on THz image by using the simulation evolutionary to obtain the edge image and non-edge image. Then the symmetric fourth order PDE is applied to non-edge image for noise removing. Finally, the edge image and noise removal image are combined to reconstruct the final de-noise image, as showed in Fig.2.

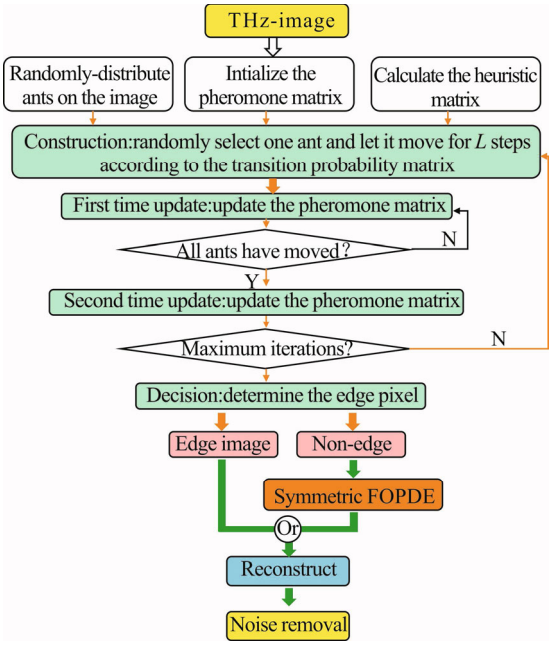

Fig.2 The diagram of the proposed method

Suppose a THz image I with size $H\times W$, $I_{i,j}$ denotes the intensity value of the pixel at the position (i, j) and let each pixel as a node, then the simulation evolutionary based edge detection can be executed according to four steps: 1) initialization, 2) construction, 3) update, and 4) decision. The details of the pseudo code are shown in Algorithm 1.

Step 1: Firstly, each component of the pheromone matrix $\tau^{(0)}$ is set to be a constant τ_{init}.

Step 2: Secondly, randomly select one ant among the total K ants at the nth construction-step, and let it consecutively move on the image for L movement-steps based on the 8-connectivity neighborhood. It moves from the node (l, m) to its neighboring node (i, j) according to a transition probability that is defined as

$$p_{(l,m)(i,j)}^{(n)}=\frac{(\tau_{i,j}^{(n-1)})^{\alpha}(\eta_{i,j})^{\beta}}{\sum_{(i,j)\in\Omega_{(l,m)}}((\tau_{i,j}^{(n-1)})^{\alpha}(\eta_{i,j})^{\beta})}, \tag{1}$$

where $\tau_{i,j}^{(n-1)}$ denotes the pheromone value of the node (i, j), $\Omega_{(l,m)}$ represents the neighborhood nodes set of the node (l, m). The constants α and β represent the influence of the pheromone matrix and the heuristic matrix, respectively. $\eta_{i,j}$, denoting the heuristic information at the node (i, j), is expressed as

$$\eta_{ij}=\frac{1}{Z}V_c(I_{i,j}), \tag{2}$$

where $Z=\sum_{i=1:M_1}\sum_{j=1:M_2}V_c(I_{i,j})$ is a normalization factor. $V_c(I_{i,j})$ is a function of a local group of pixels c (called the clique), and its value depends on the variation of image's intensity values on the clique c. For example, it can be defined as

$$V_c(I_{i,j}) = f(|I_{i-2,j-1} - I_{i+2,j+1}| + |I_{i-2,j+1} - I_{i+2,j-1}| + |I_{i-1,j-2} - I_{i+1,j+2}| + |I_{i-1,j-1} - I_{i+1,j+1}| + |I_{i-1,j} - I_{i+1,j}| + |I_{i-1,j+1} - I_{i-1,j-1}| + |I_{i-1,j+2} - I_{i+1,j-2}| + |I_{i,j-1} - I_{i,j+1}|) . \quad (3)$$

Here we adopt a parameter γ to adjusts the functions' respective shapes and the function $f(\cdot)$ in Eq.(4) can be determined as

$$f(x) = \begin{cases} \dfrac{\pi x \sin(\dfrac{\pi x}{\gamma})}{\gamma}, & 0 \le x \le \gamma \\ 0, & \text{else} \end{cases} . \quad (4)$$

Step 3: Thirdly, performs two update operations for the pheromone matrix. One is conducted after the movement of each ant within each construction step according to

$$\tau_{i,j}^{(n-1)} = \begin{cases} (1-\rho)\tau_{i,j}^{(n-1)} + \rho\Delta_{i,j}^{(k)}, & \text{if } (i,j) \text{ is visited} \\ & \text{by the current } k\text{th ant} \\ \tau_{i,j}^{(n-1)}, & \text{otherwise} \end{cases} , \quad (5)$$

where ρ is the evaporation rate, $\Delta_{i,j}^{(k)}$ is determined by the heuristic matrix $\Delta_{i,j}^{(k)} = \eta_{i,j}$.

The other is carried out after the movement of all ants within each construction step according to

$$\tau^{(n)} = (1-\psi)\cdot\tau^{(n-1)} + \psi\cdot\tau^{(0)}, \quad (6)$$

where ψ is the pheromone decay coefficient.

Then the ant movement operation has been run for N iterations to construct the final pheromone matrix $\tau^{(N)}$ by iteratively performing both the construction process and the update process.

Step 4: Finally, a binary decision process is performed to determine the edge based on threshold T,

$$T^{(l)} = \frac{m_L^{(l)} + m_U^{(l)}}{2} . \quad (7)$$

The initial threshold $T^{(0)}$ is selected as the mean value of the pheromone matrix. Next, the entries of the pheromone matrix is classified into two categories according to the criterion that its value is lower than $T^{(0)}$ or larger than $T^{(0)}$. Then the new threshold is computed as the average of two mean values of each of above two categories. The above process is repeated until the threshold value does not change any more.

Recently, the symmetric fourth order PDE has been applied for image denoising due to it can reduce the block effects existed in second-order PDE[16]. The classical PDE is based on minimize the total variation[17] defined as

$$\min_{u \in BV(\Omega) \cap L^2(\Omega)} \int_\Omega |Du| + \frac{\lambda}{2}\int_\Omega (u-u^0)^2 \mathrm{d}x , \quad (8)$$

where Ω represents an open domain with a Lipschitzian boundary, u and u^0 denote the original image and the observed image respectively, λ is an adjust parameter depended on the specific application.

Algorithm 1 The pseudo code of the simulation evolutionary

Input: K the total number of ants.
N the total number of construction-steps.
α the weighting factor of the pheromone information.
β the weighting factor of the heuristic information.
Ω the connectivity neighborhood.
γ the adjusting factor.
τ_{init} the initial value of each component of the pheromone matrix.
P the evaporation rate.
ψ the pheromone decay coefficient.
L total number of ant's movement-steps within each construction-step.
Output: Detect the image edge.
Initialize the pheromone matrix $\tau^{(0)} \leftarrow \tau_{\text{init}}$;
for $n \leftarrow 1$ **to** N **do**
  for $k \leftarrow 1$ **to** K **do**
    Randomly select one ant (k);
    Consecutively move the ant(k) for L steps according to Eq.(1) ;
    if position (i, j) is visited by ant(k)
      update the pheromone matrix $\tau^{(n)}$ based on Eq.(5);
    end
  end
  if all the ants have visited position (i, j)
    update the pheromone matrix $\tau^{(0)}$ based on Eq.(6);
  end
end
Adaptively compute the threshold T according to Eq.(7);
Make the solution decision with threshold T on the final pheromone matrix $\tau^{(N)}$;
return;

In fact, to smooth an image u and keep the u approaches to u^0 can be transferred to an optimization problem by finding a minimum $|\nabla^2 u|$, that is minimize the energy function

$$E(u) = \iint_\Omega (f(|\nabla^2 u|) + \frac{\lambda}{2}|u-u^0|^2)\mathrm{d}x\mathrm{d}y , \quad (9)$$

where ∇^2 denotes Laplacian operator and $f(\cdot)>0$ is an increasing function. Then, a Euler-Lagrange equation $\nabla^2(f'(|\nabla^2 u|)sign(|\nabla^2 u|)) + \lambda(u-u^0) = 0$ can be obtained, *sign* represents the sign function. Therefore, $\nabla^2(f'(|\nabla^2 u|)\dfrac{\nabla^2 u}{|\nabla^2 u|}) + \lambda(u-u^0) = 0$ can be finally gained. Let $c(s) = \dfrac{f'(s)}{s}$, the former equation can be written as

$$\nabla^2(c(|\nabla^2 u|)\nabla^2 u) + \lambda(u-u^0) = 0 . \quad (10)$$

To solve the above Euler-Lagrange equation, the time

t and gradient descent method are introduced as

$$\frac{\partial u}{\partial t} = -\nabla^2(c(|\nabla^2 u|)\nabla^2 u) - \lambda(u - u^0) . \quad (11)$$

Finally, discretization iterative can be used to solve the above equation.

To simplify and symmetry the discretization result, a simple symmetric difference program base on the four field structure (as shown in Fig.3) is proposed in this paper to solve the equation by discretization iterative.

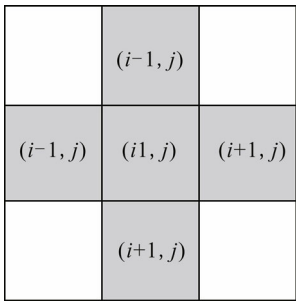

Fig.3 the symmetric field structure

For the central point, $\nabla^2 u$ can be discretized as

$$\nabla^2 u|_{i,j} = \frac{u_{i+1,j} + u_{i-1,j} + u_{i,j+1} + u_{i,j-1} - 4u_{i,j}}{h^2} , \quad (12)$$

where h is the discretization space step. Then we can obtain the iterative formula

$$u^{n+1} = u^n - \Delta t(\nabla^2(c(|\nabla^2 u^n|)\nabla^2 u^n) + \lambda(u^n - u^0)) , \quad (13)$$

where Δt denotes the discretization time step. Similarly to the Ref.[16], we can make $c(s)$ as follows:

$$c(s) = \frac{1}{1 + (s/k)^2} , \quad (14)$$

where k is a parameter.

Thus, the symmetric fourth order PED based denoising can be conducted according to the following steps:

1) Initialize the parameters λ, k, h, Δt and the original image u;

2) Compute $\nabla^2 u$ and $|\nabla^2 u|$ by Eq.(12);

3) Calculate $c(|\nabla^2 u|)$ by Eq.(13);

4) Iterate via Eq.(14);

5) If not reach the maximum iteration, then go to step 2), else end.

To conduct the experiments, the Spectra Physics Hurricane (output wavelength is 800 nm, repetition frequency is 1 kHz, single pulse energy is 900 μJ and pulse width is 120 fs) is selected as a laser source. CCD camera as the detector can obtain the real-time image of object. The measured object is placed in the 2D scanning step platform with positioning accuracy of 1 μm.

Three kinds of THz images are adopted for comparison experiment: covered mosaic 128×128[18], hidden toy gun 128×128, and double forks 128×128[19]. At the same time, three different methods, Donoho threshold, generalized wavelet threshold, and adaptive thresholding, are selected for comparison. The denoising approaches are implemented with the Matlab programming language and run on a PC with a i5-2400 3.1 GHz CPU and a 4 096 MB RAM, One hundred experiments are conducted for each of the above-mentioned approaches.

Because the algorithm is a typical probabilistic algorithm, the parameters in the algorithm are usually determined by experimental methods.

In this paper, the simulation experiment selects the representative eil51 in the TSPLIB standard library as the test object.

The steps of parameter simulation test are as follows:

(1) Set the initial value of the parameter and set the default value of each parameter. (the scale of this simulation experiment is 50).

(2) Keep the default values of β and ρ unchanged, α increases with a step size of 0.1 from 0, and the experiment is repeated 100 times each time, and the optimal value is obtained.

(3) Keep the default values of α and ρ unchanged, β increases step by step from 0 to 0.1, and the experiment is repeated 100 times each time, and the optimal value is obtained.

(4) Keep the default values of α and β unchanged, ρ increases step by step from 0 to 0.1, and the experiment is repeated 100 times each time, and the optimal value is obtained.

(5) Other parameters can be calculated from Eqs.(4) and (5).

(6) Based on the comprehensive analysis of the experimental data obtained under the combination of various parameters mentioned above, the best value range of each parameter and the combination and optimization setting among the parameters are summarized.

In addition, the parameters involved in the proposed methods are given in Tabs.1 and 2.

Tab.1 Parameter setting for edge detection method with simulation evolutionary

Parameter	Value	Parameter	Value
α	1	γ	1
β	0.1	ρ	0.1
Ω	8	L	40
τ_{init}	0.001	ψ	0.05
N	4	K	$\sqrt{H \times W}$

Tab.2 Parameter setting for symmetric fourth order PDE

Parameter	Value	Parameter	Value
h	1.2	λ	1
k	1	Δt	0.2

Firstly, the proposed method is compared with the other three approaches mentioned above on three different THz images. Figs.4—6 illustrate the experiment results. It can be concluded that the Donoho threshold and the

generalized wavelet threshold perform worse owing to they will lose some useful information. In addition, our proposed approach and the adaptive thresholding posses better denosing effects than the other two methods. Furthermore, our proposed approach performs better than the adaptive thresholding method.

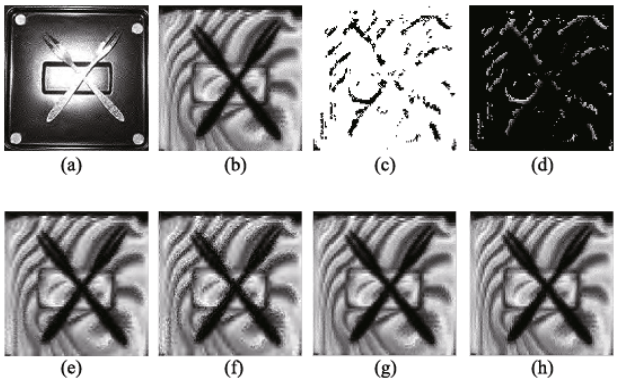

Fig.4 Various results of double fork: (a) Optical image; (b) THz image of double fork; (c) Edge image of double fork THz image; (d) Non-edge image of double fork THz image; (e) Denoised image by Donoho threshold; (f) Denoised image by generalized wavelet threshold; (g) Denoised image by adaptive thresholding; (h) Our proposed approach

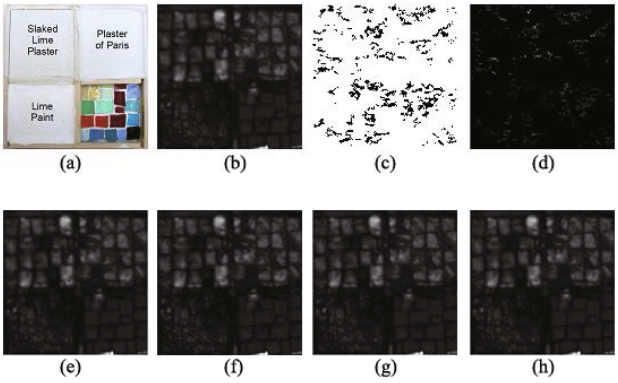

Fig.5 Various results of covered mosaic: (a) Optical image; (b) THz image of covered mosaic; (c) Edge image of covered mosaic THz image; (d) Non-edge image of covered mosaic THz image; (e) Denoised image by Donoho threshold; (f) Denoised image by generalized wavelet threshold; (g) Denoised image by adaptive thresholding; (h) Our proposed approach

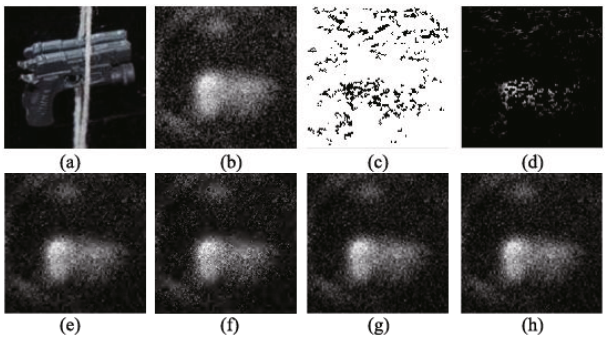

Fig.6 Various results of hidden toy gun: (a) Optical image; (b) THz image of hidden toy gun; (c) Edge image of hidden toy gun THz image; (d) Non-edge image of hidden toy gun THz image; (e) Denoised image by Donoho Threshold; (f) Denoised image by Generalized Wavelet Threshold; (g) Denoised image by adaptive thresholding; (h) Our proposed approach

Furthermore, the mean squared error (*MSE*), the signal-to-noise ratio (*PSNR*), the root mean square (*RMS*) and the normalized mean square error (*NMSE*) are explored on the de-noise results by using these methods. In addition, the computational complexity (run time) of the proposed approach compared with other four methods is also conducted.

$$MSE = \frac{1}{mn}\sum_{i=0}^{m-1}\sum_{j=0}^{n-1}\| u_{ij} - u_{ij}^{\ 0} \|^2, \tag{15}$$

$$PSNR = 10 \cdot \log_{10}(\frac{MAX^2}{MSE}), \tag{16}$$

$$RMS = \sqrt{\frac{1}{mn}\sum_{i=0}^{m-1}\sum_{j=0}^{n-1}\| u_{ij} - u_{ij}^{\ 0} \|^2}, \tag{17}$$

$$NMSE = \frac{1}{sumx}\sum_{i=0}^{m-1}\sum_{j=0}^{n-1}|u_{ij} - u_{ij}^{\ 0} \|^2, \tag{18}$$

where MAX is the largest value of image point, $sumx = \sum_{i=0}^{m-1}\sum_{j=0}^{n-1} u_{ij}^{\ 0}$, and the unit of *PSNR* is dB.

From Tab.3, it can be observed that the MSE, NMSE and RMS of our proposed approach are smallest amongall the methods, i.e. the difference between the de-noise image and the original image is smaller. What's more, the *PSNR* of our proposed approach is the largest one among the four models, which means that our proposed approach can preserve the edge information to a large extent when removing the noises. Therefore, experimental results reveal that our model performs better in THz image de-noise than the other three models.

Tab.3 The performance comparison on *PSNR*, *MSE*, *NMSE*, *RMS* and run time

Methods	*PSNR* (dB)	*MSE*	*NMSE*	*RMS*	Run time (s)
Test image of covered mosaic					
Donoho	39.474 0	$1.145\ 4\times10^{-4}$	$7.857\ 0\times10^{-4}$	$1.070\ 2\times10^{-2}$	0.038
Generalized wavelet	38.225 7	$1.506\ 0\times10^{-4}$	$1.033\ 0\times10^{-3}$	$1.227\ 2\times10^{-2}$	0.021
Adaptive thresholding	49.164 3	$1.164\ 7\times10^{-5}$	$7.989\ 1\times10^{-5}$	$3.412\ 7\times10^{-3}$	0.092
Our proposed approach	67.644 6	$1.718\ 4\times10^{-7}$	$1.178\ 7\times10^{-6}$	$4.145\ 3\times10^{-4}$	0.036
Test image of toy gun					
Donoho	30.176 6	$8.500\ 4\times10^{-4}$	$5.259\ 3\times10^{-3}$	$2.915\ 6\times10^{-2}$	0.038

Generalized wavelet	27.182 5	$2.019\ 6\times10^{-3}$	$1.249\ 6\times10^{-2}$	$4.494\ 1\times10^{-2}$	0.020
Adaptive thresholding	41.186 2	$6.841\ 1\times10^{-5}$	$4.232\ 7\times10^{-4}$	$8.271\ 1\times10^{-3}$	0.110
Our proposed approach	45.425 5	$2.584\ 9\times10^{-5}$	$1.599\ 3\times10^{-4}$	$5.084\ 2\times10^{-3}$	0.036
Test image of double fork					
Donoho	28.460 1	$1.703\ 2\times10^{-3}$	$3.349\ 4\times10^{-3}$	$4.127\ 0\times10^{-2}$	0.038
Generalized Wavelet	25.687 8	$3.635\ 3\times10^{-3}$	$7.148\ 8\times10^{-3}$	$6.029\ 4\times10^{-2}$	0.020
Adaptive thresholding	34.956 6	$3.715\ 8\times10^{-4}$	$7.307\ 1\times10^{-4}$	$1.927\ 6\times10^{-2}$	0.090
Our proposed approach	36.577 4	$2.335\ 6\times10^{-4}$	$4.593\ 0\times10^{-4}$	$1.528\ 3\times10^{-2}$	0.037

THz image have aroused great interests on biomedicine, measurement and detection. However, background noises normally present in THz images caused by the THz pulse coherent superposition in detector. To enhance the image quality, simulation evolutionary and symmetric fourth order PDE have been combined. Experiments on three different THz images prove that the proposed method compared with other three methods can largely reduce noises and preserve the edge information.

Our future work will focus on the segmentation of THz images.

References

[1] J. Liu and Z. Li, Optik-International Journal for Light and Electron Optics **125**, 3423 (2014).

[2] Jie Li, Jitao Li, Yue Yang, Jining Li, Yating Zhang, Liang Wu, Zhang Zhang, Maosheng Yang, Chenglong Zheng, Jiahui Li, Jin Huang, Fuyu Li, Tingting Tang, Haitao Dai and Jianquan Yao, Carbon **163**, 34 (2020).

[3] A. Jolly, F. S. Gokhan, J. C. Jolly, S. Hocquet and B. Chassagne, Applied Physics B-Lasers and Optics **120**, 441 (2015).

[4] J. Bianca Jackson, Julien Labaune, Rozenn Bailleul-Lesuer, Laura D'Alessandro, Alison Whyte, John W. Bowen, Michel Menu and Gerard Mourou, Frontiers of Optoelectronics **8**, 81 (2015).

[5] S. Yassin, K. Su, L. F. Gladden and J. A. Zeitler, Journal of Pharmaceutical Sciences **104**, 1658 (2015).

[6] M. Kulya, N. V. Petrov and V. Katkovnik, Applied Optics **58**, 5533 (2019).

[7] M. H. Balgos, R. Jaculbia and E. A. Prieto, Journal of Applied Physics **126**, 3494 (2019).

[8] C. H. Shon, W. Y. Chong, S. G. Jeon, G. J. Kim, J. I. Kim and Y. S. Jin, J. Infrared and Millimeter Waves **29**, 79 (2008).

[9] Wang Nan, Zhang Xiaoxuan and Liang Jie, Journal of Physics D-Applied Physics **29**, 53 (2020).

[10] Bassli Amine, Blin Stephane and Nouvel Philippe, IEEE Transactions on Instrumentation and Measurement **69**, 5843 (2020).

[11] Buades A, Coll B and Morel J, A Non-Local Algorithm for Image Denoising, IEEE-International Conference on Computer Vision and Pattern Recognition, 60 (2005).

[12] You Yuli and Kaveh M, IEEE Transactions on Image Processing **9**, 1723 (2000).

[13] Benhamza K, Merabti H and Seridi H, Adaptive Edge Detection Using Ant Colony, 8th International Workshop on Systems, Signal Processing and their Applications (WoSSPA), 197 (2013).

[14] C. Pereira, L. Goncalves and M. Ferreira, Medical & Biological Engineering & Computing **51**, 295 (2013).

[15] M. Dorigo, M. Birattari and T. Stutzle, IEEE Computational Intelligence Magazine **1**, 28 (2006).

[16] Y. L. You and M. Kaveh, IEEE Transactions on Image Processing **9**, 1723 (2000).

[17] R. C. Gonzalez and R. E. Woods, Digital Image Processing (Second edition), Prentice Hall, Upper Saddle River, NJ, 2002.

[18] J. Bianca Jackson, Julien Labaune, Gérard Mourou, Irl Duling, Gillian Walker, J. W. Bowen and Michel Menu, Terahertz Pulse Imaging of Stratified Architectural Materials for Cultural Heritage Studies, Proceedings of SPIE - The International Society for Optical Engineering, O3A: Optics for Arts, Architecture, and Archaeology III, Munich, Germany, 8084 (2011).

[19] JIANG Tian, SHEN Huiliang, YANG Dongxiao, LIU Jianjun and ZOU Zhe, Laser Technology **39**, 289 (2015).